International Journal of Precision Engineering and Manufacturing-Green Technology (2026) 13:1921–1934
https://doi.org/10.1007/s40684-025-00782-5

Online ISSN 2198-0810
Print ISSN 2288-6206

REGULAR PAPER

Acoustofluidics Lab on a Chip System for size-based Nanoparticle Separation

Jaeyun Yoon[1] · Noori Kim[1,2] · Saeeun Jang[4] · Jinhong Noh[4] · Inkyu Park[4] · Suhan Lee[4] · Hae-Jin Choi[3] · Yong-Jin Yoon[1,4]

Received: 8 May 2025 / Revised: 20 August 2025 / Accepted: 24 August 2025 / Published online: 10 September 2025
© The Author(s) 2025

Abstract

Despite the growing demand for nanoscale biomolecule analysis in point-of-care (POC) applications, nanoparticle separation remains a significant challenge. This is due to issues like high sample loss, low throughput, large-scale material requirements, and the complexity of current technologies. Given that separation efficiency directly impacts subsequent sample processing and analysis, there is a clear need for a robust and reliable size-based separation technique. This study introduces a novel acoustofluidics lab-on-a-chip system designed to overcome current separation barriers. It combines simple polymer prototyping with integrated ultrasonic agitation. The system features two key components: (1) a microfluidic network embedded with membrane filters of varying pore-size cut-offs, and (2) an ultrasonic transmitter that induces acoustic agitation. Using this novel system, we successfully demonstrate the fractionation of 60 nm Au nanoparticles from a polydisperse solution under ultrasonic waves (28–40 kHz) generated by the transducer integrated into the microfluidic platform. Ultrasonic irradiation not only prevents cake formation but also reverses the fouling process through acoustic agitation. This significantly increases the flow rate during separation and improves the recovery of target-size nanoparticles. This microfluidic platform holds great potential as a powerful tool for sample preparation and analytical methodologies in POC applications.

Keywords Acoustofluidics · Nanoparticle separation · Point-of-care (POC) application · Lab on a chip (LOC) system · Ultrasonic irradiation · Acoustic agitation.

1 Introduction

With the growth in microfluidic technologies in the COVID-19 era, a substantial advance in the Lab-on-a-Chip (LOC) system has been presented, enabling miniaturization and integration of complex functions routinely performed by hand in the traditional analytical processes [1–3]. One of the most active applications of the LOC is observed in biomedical research with Point-of-care (POC) diagnostic devices. The POC diagnostic system can rapidly deliver diagnostic outcomes to patients, providing the users with many benefits over the traditional diagnostic methods, such as a straightforward and easy-to-use interface, portability, less sample and reagent consumption, etc [4].

In biomedical research, size-based particle separation plays a significant role in the sample preparation process and the detection of target species [5, 6]. As the size of analytes in biological research ranges from angstrom to millimeter scale, the separation mechanism of choice depends on

✉ Hae-Jin Choi
hjchoi@cau.ac.kr

✉ Yong-Jin Yoon
yongjiny@kaist.ac.kr

1 School of Mechanical and Aerospace Engineering, Nanyang Technological University (NTU), Singapore 639798, Singapore

2 School of Engineering Technology, Purdue University, West Lafayette, IN 47907, USA

3 School of Mechanical Engineering, Chung-Ang University, Seoul 06974, Republic of Korea

4 Department of Mechanical Engineering, Korea Advanced Institute of Science and Technology (KAIST), Daejeon 34141, Republic of Korea

their dimensions. During the past decade, many size-based separation techniques have been established for biomedical applications [6, 7]. Enormous progress has been made, and size-based separation technologies are moving towards miniaturized platforms to meet the requirements for point-of-care testing. Many detection techniques require isolating target species of interest from solutions during sample preparation to provide unbiased and accurate insights into the biological process or phenomena. Since the dimension of biological structures ranges from angstrom to millimeter scale, the separation method varies depending on the target size due to the growing need for robust and reproducible size-based particle separation techniques. Especially, significant efforts have been put into developing a miniaturized size-selective particle sorting method for point-of-care applications such as LOC particle sorters [8–10]. However, the LOC-based separation techniques are limited to the submicron scale (such as cells, viruses, and bacteria), which results in significant sample loss, diagnostics misinterpretation, and poor detection limit [11–14]. Developing robust and reliable size-based particle separation techniques is emerging as an essential prerequisite for nanoscale measurement to obtain insights into the various biological systems on a nanometer scale.

For nanoscale biomolecule sorting, biomedical research has carried out several size-dependent nanoparticle separation techniques such as technology based on external fields application, physical sieving, and size-selective precipitation. Unfortunately, commonly used current technologies for NP separation were still not sufficiently efficient in selectively sorting particles based on their size or molecular weight for proper POC use due to their complex hands-on processes and incompatibility with downstream analytical devices. A miniaturized, compact, cost-effective platform for size-based separation is more favorable than one in centralized laboratories to eliminate the need for bulky and sophisticated instruments and extensive input material and minimize the complexity of the device's operation.

For nanoscale biomolecule separation, several size-dependent nanoparticle separation techniques have been employed. Based on the separation mechanism, these techniques fall into three categories: the use of external fields (centrifugal [15–17], electrical [18–20] and magnetic [21, 22]), physical barriers for sieving [23], and size-dependent precipitation [24]. One of the most widely used methods based on the application of external fields is field flow fractionation (FFF). FFF is a particle separation technique that takes advantage of the field exerted on a solution flowing through a channel. The field is perpendicular to the fluid flow, which results in the separation of particles suspended in the carrier solution due to the difference in travelling speed depending on their size and molecular weight. Despite its variations and versatility, it has not been widely used as a size based nanoparticle separation method due to its low throughput and extensive input material required. Alternatively, a size-dependent precipitation method has been devised. Size-dependent precipitation occurs when the stability, physical or chemical properties change depending on the surface chemistry of the nanoparticles. Sieving is another alternative for the size-selective fractionation of nanoparticles. Chromatography and membrane filtration employs physical barriers such as a column or physical hole to control elution and retention depending on the size of particles. Unfortunately, these traditional size-based nanoparticle separation techniques result in huge sample loss, therefore, large input material is required. In addition, bulky instrumentation is involved in generating external field during the separation process. Due to the complexity of these technologies, there has been increasing demand for the development of miniaturized and compact platform for size-based separation, which can be used as a cost-effective preparative method in point of care application.

There have been many microfluidic approaches to bring the size-selective nanoparticle separation into miniaturized platforms. One of the most common separation mechanisms utilized in the microfluidic platform is membrane-based filtration because of its high resolution and straightforward procedure [25–28]. Gaborski et al. [23] demonstrated nanoparticle fractionation using porous nanocrystalline silicon membranes with resolution as high as 5 nm, potentially applicable to Lab-on-a-Chip system for dead-end filtration. However, membrane filtration typically suffers from low efficiency associated with clogging and formation of cake layer near membrane filter [29], leading to low flow rate, sample loss, and high fluid resistance [30]. Also, the fabrication of nanopores involves a complicated and time-consuming micro-fabrication process due to nanoscale particle separation. To circumvent this limitation, "filter-free" microfluidic separation techniques have been developed. Microfluidic approaches based on electrophoresis, field-flow fractionation (FFF) [31, 32] and centrifugation [15–17] have been devised and implemented for size-based nanoparticle separation and fractionation. However, these techniques still rely on external fields which usually need the bulky instrument to manipulate particle motion.

Furthermore, most passive separation techniques necessitate expensive microfabrication. For point-of-care applications, a lab-on-chip system is required that can be realized through a simple fabrication process, offers a user-friendly interface for easy sample handling, and yet achieves high resolution with minimal sample loss [33–35]. For these reasons, the lack of reliable size-selective nanoparticle separation is a bottleneck in analyses of nanoscale biomolecules

such as ribosome profiling, which requires size-selective separation of monosomes from polysome molecules [36].

Acoustofluidics can be effectively employed in membrane filtration, offering straightforward processing with high resolution and several advantages over filter-free alternatives. When acoustic signals, such as pure tone waves, interact with materials, they often produce fascinating patterns, phenomena, or results. In 1787, Chladni famously visualized sound frequencies or vibrations using sand sprinkled on glass plates, creating what are now known as Chladni figures [37]. Since then, acoustic waves have been integrated into various fields to achieve contactless processes across scales, from macroscale to microscale.

When acoustic waves are employed to manipulate fluids or particles at the micro- and nanoscale, the field is known as acoustofluidics. Its applications are vast, spanning from fundamental physics to advanced engineering [38, 39]. While it is unclear who first coined the term "acoustofluidics," it appears to have emerged from collaborative research efforts in the mid-2000s, led by Dr. Huang [40, 41]. Many studies have explored how acoustofluidics can enhance membrane filtration, particularly through ultrasonic treatment of membrane filters. However, most of this research has focused on bulk processing for industrial applications, such as wastewater treatment, food processing, and ultrapure water production [42, 43]. These typically involve ultrasonic baths, which, while effective, require high energy consumption and large quantities of input material, making them less suitable for biological applications where input material may be limited. To achieve simple and rapid size-selective nanoparticle separation for point-of-care (POC) applications, we have developed an acoustofluidics lab-on-a-chip (LOC) system that incorporates commercially available track-etched membrane filters with varying pore-size cut-offs, enabling effective dead-end filtration. We processed samples containing polydisperse nanoparticles on this microfluidic platform, which is equipped with embedded membrane filters. However, dead-end filtration often faces challenges such as clogging and membrane fouling due to the formation of a cake layer near the membrane surface, resulting in reduced flow rates and potential membrane and sample loss. To address this, we integrated ultrasonic transmitters with the membrane filtration system, enabling online ultrasonic treatment. This ultrasonic-assisted membrane filtration was adapted to fit within a miniaturized microfluidic platform. The functionality of this novel LOC technology was validated through the successful size-based separation of gold and polymer nanoparticles. The following chapters detail our system design methods, followed by results and discussion.

2 Experiment

2.1 Basic Principles of dead-end Membrane Filtration

In dead-end membrane filtration, the input fluid flow, known as the "feed" solution, is typically directed perpendicular to the membrane surface. Driven by pressure within the filtration system, a portion of this fluid passes through the membrane pores, becoming the "filtrate" or "permeate." Meanwhile, another portion of the fluid remains on the membrane surface, referred to as the "retentate." To evaluate the performance of membrane-based filtration, the permeate and retentate are collected separately and analyzed using various methods. When the target nanoparticles are metals such as gold or silver, absorbance measurement is one effective way to quantify filtration performance. For small gold nanoparticles (~30 nm), the surface plasmon resonance effect causes an absorption maximum at a wavelength of 526 nm. For larger gold nanoparticles (~60 nm), the absorption maximum shifts to 540 nm. By measuring the absorbance of the collected filtrate and retentate samples, the proportion of target-size nanoparticles in each sample can be determined. These absorbance measurements then provide a basis for assessing the performance of the dead-end membrane filtration system.

2.2 Working Principle of ultrasonic-assisted Nanoparticle Separation

The working principle of ultrasonic-assisted nanoparticle separation on a microfluidic device is illustrated in Fig. 1. The separation mechanism relies on a straightforward dead-end filtration process. The microfluidic system designed for size-based nanoparticle separation consists of a microfluidic device integrated with track-etched polycarbonate membrane filters, which have sharp pore size cut-offs, and an ultrasonic transducer. To isolate monodisperse nanoparticles from a mixture, membrane filters with pore sizes slightly larger and smaller than the target particle size are employed.

As depicted in Fig. 1, target particles (shown in green) pass through the membrane with a larger cut-off value, while larger particles are retained on the membrane surface. A second membrane with a smaller cut-off is then used to capture the target particles, allowing for their purification before collection. Impurities and particles smaller than the target size flow through the second membrane and are directed to the waste reservoir.

One of the critical limitations in dead-end filtration is sample loss and decrease in permeability during the separation process due to particle adsorption on the membrane surface and the formation of a cake layer near the surface.

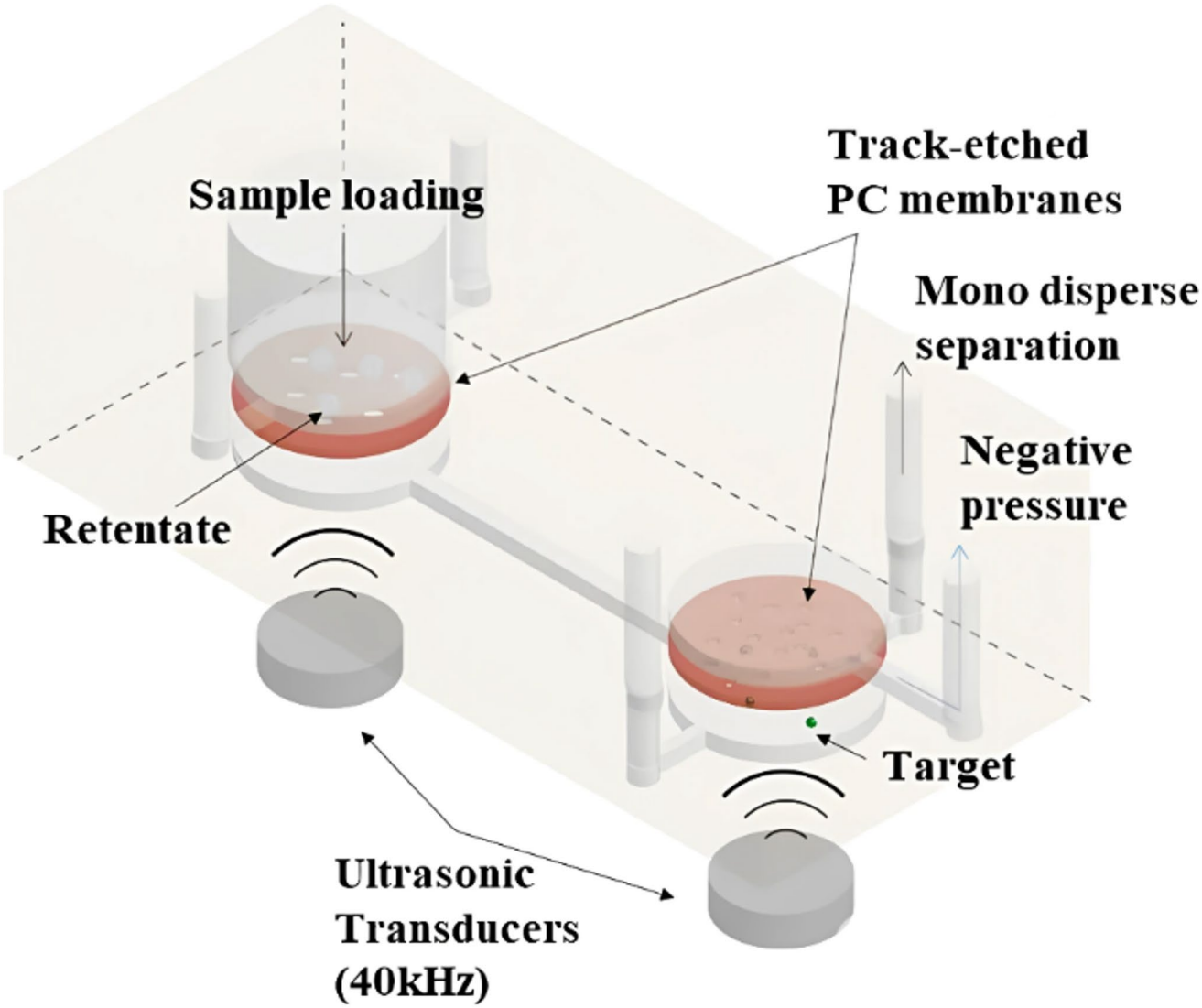


Fig. 1 Schematic of a microfluidic platform for nanoparticle separation

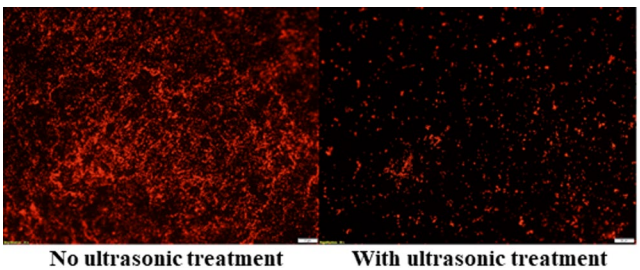


Fig. 2 Effect of ultrasonic treatment during NP separation

An ultrasonic wave was exploited to detach fouled particles on the surface and enhance the target recovery of particles. (Fig. 2) The transducer was located near the membranes for efficient ultrasound irradiation to minimize the attenuation as the wave propagates through the material. And the chamber was designed to fit the active area of the transducer to maximize the coverage of ultrasound irradiation. Negative pressure was applied through the outlet to prevent leakage at the interface of the PDMS layer and the membranes.

2.3 Chip Design and Fabrication

The microfluidic nanoparticle separation device prototype was designed using AutoCAD software and constructed by a standard soft lithography process. The device consists of two circular reservoirs connected by a microfluidic network to filtrate nanoparticles, as illustrated in Fig. 3. The microfluidic network patterned onto the bottom layer, which connects the two reservoirs. The side channels connected to the reservoir for sample collection are patterned onto the middle layer. And the top layer serves as a top cover to form a closed microfluidic network while the left reservoir remains

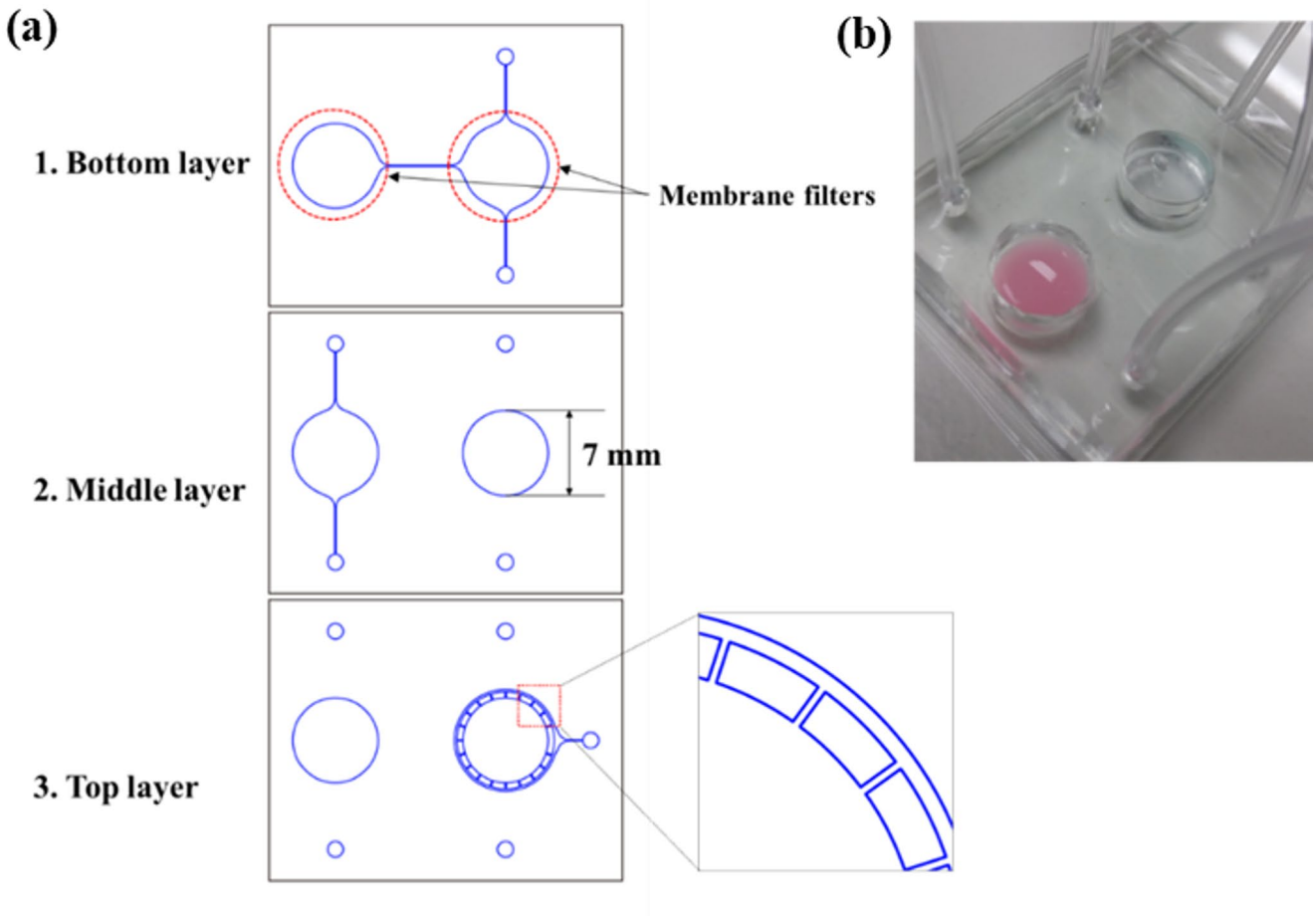


Fig. 3 Fabrication of microfluidic nanoparticle separation device. (a) Each PDMS layer was patterned by standard soft lithographic technique. Using an uncured PDMS prepolymer, membrane filters were embedded in the interface between the bottom and middle layers. The left reservoir served as a sample loading well. (b) A microfluidic nanoparticle separation device with a sample loaded in a sample reservoir

open for sample loading. The right reservoir has microfluidic barrier structures to guide the fluid flow uniformly to cover the entire surface of the membrane, and it enables the even distribution of the particles to infiltrate the membrane surface.

The left reservoir serves as a sample loading well where a mixture of nanoparticles was loaded. The membrane filters with different pore sizes were integrated with three PDMS layers in the NP separation process. First, the structures of each PDMS layer were patterned onto a transparency mask and supplied by Fineline Imaging (Colorado Springs, CO) at 32,000 dpi resolution. To fabricate a master mold, SU-8 2025 was spun onto a silicon substrate using a spin coater at 2000 rpm for 30 s to achieve a uniform thickness of 40 µm. Then the master went through a soft bake process to evaporate solvent at 65 °C for 2 min and 95 °C for 5 min followed by UV exposure (200 mJ/cm^2) for 30 s. For Post-exposure bake (PEB), the master was cured at 65 min for 1 min and 95 min 3 min. Then the pattern was developed by immersing the master in the developer solution for 5 min and rinsing with Deionized water and isopropyl alcohol.

Excess water must be removed in a spin dryer. After the patterning process, the SU-8 mold was modified with trimethylchlorosilane (Sigma-Aldrich, USA) under vacuum. Next, the PDMS layers were fabricated by standard soft lithographic techniques. Briefly, PDMS was mixed with a curing agent at a ratio of 10:1, and it poured onto the SU-8 master mold to form a replica of the device. Degassing was performed to remove entrapped bubbles from the layer. Then the layer was baked in a convection oven at 65 °C for an hour for curing and peeled off from the master mold. Two reservoir regions were punched with biopsy punches, and holes at the inlet and outlet were punched for fluidic access.

Membrane filters were cut using the laser cutting process into the desired size. Pore sizes of membrane filters varied depending on the target nanoparticle size. Uncured elastomer/curing agent mixture was applied along the reservoir's edge to integrate the membrane filter on the PDMS bottom

layer. Then the membrane was aligned, placed at the center of the reservoir, and pressed gently with a round tip tweezer to absorb the uncured mixture into the filter layer. The bottom layer and membrane filter were cured in an oven at 65 °C for at least 30 min. Three PDMS layers were oxygen plasma treated to activate the surface, aligned and brought into contact with each other to form a microfluidic platform. Tygon tubings were inserted into through holes at inlets and outlet regions. After integration and assembly, no significant leak was observed during operation. SU-8 master mold can be reused after washing with IPA and deionized water. The microfluidic device was coupled with ultrasonic transducers by using silicone at the interface of the transducer and PDMS layer to minimize the energy loss and attenuation during operation.

2.4 Ultrasonic Assisted Nanoparticle Separation on a Microfluidic Device

The overall experiment set up is shown in Fig. 4 (a), a 40 kHz square wave was developed by a function generator and 50 times amplified through a high voltage amplifier (WMA-300, Falco systems) and used to excite the ultrasonic transducer. Before separation, the microfluidic network was rinsed with 0.1% Poly(ethylene glycol)-*block*-poly(propylene glycol)-*block*-poly(ethylene glycol) (Pluronic F108)(Sigma-Aldrich) solution to remove residual impurities and treat

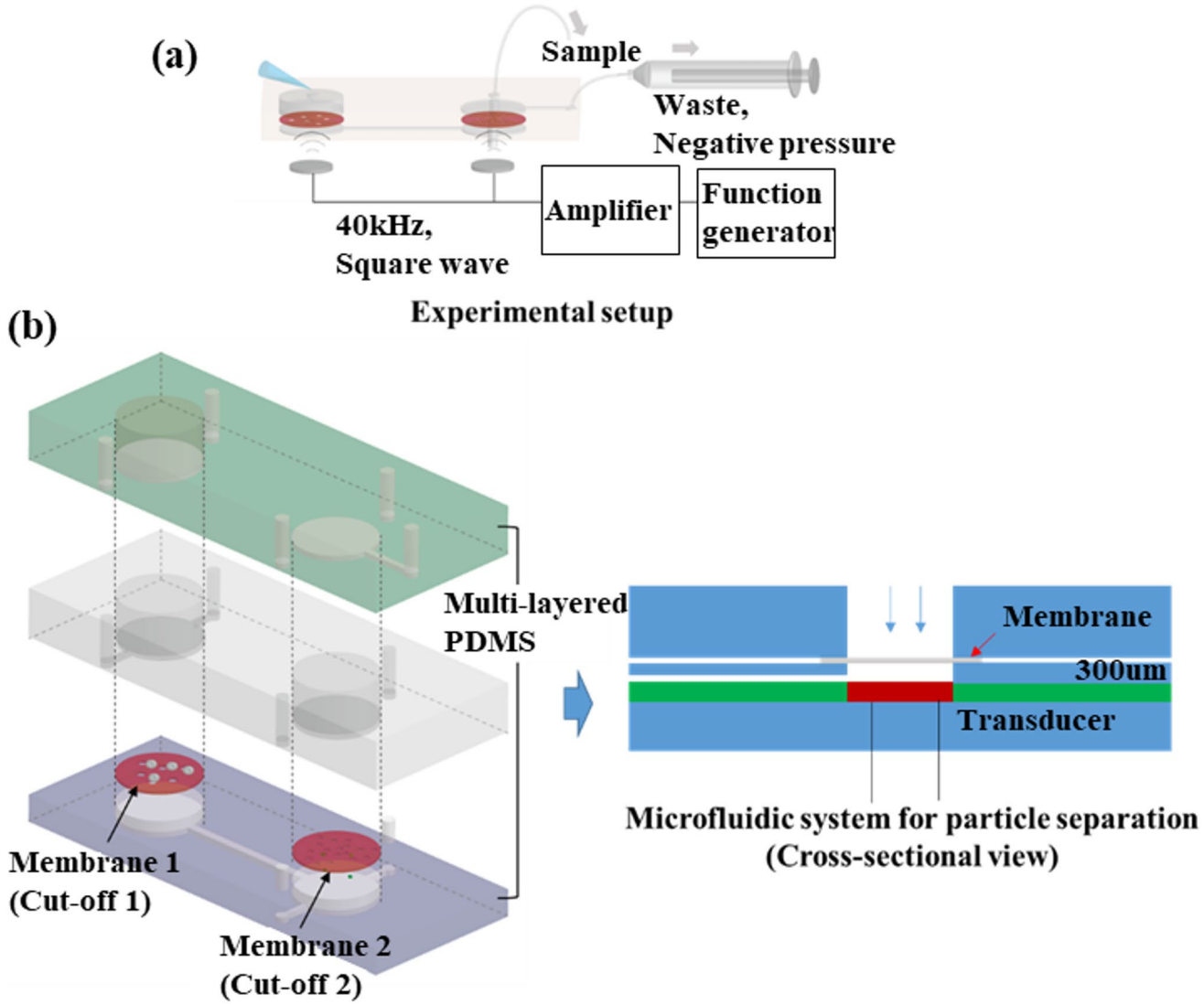


Fig. 4 Microfluidic device for on-chip nanoparticle separation consists of three PDMS layers. (**a**) Over all experimental setup (**b**) Membrane filters with different cut-off sizes (Cut-off 1 and Cut-off 2) were sandwiched between the bottom and middle layers for two different sizes nanoparticle separation. Particles larger than the cut-off of the first membrane remain in the sample loading reservoir, and the rest can penetrate the membrane. Particles and buffer solution can go through the second membrane with a smaller cut-off (Cut-off 1), while the target size particle (Cut-off 2) stay in the chamber region between those two membrane filters

the fluidic PDMS surface, thereby preventing adsorption of nanoparticle on the membrane surface or fluidic channel wall and formation of fouling on the membrane surface. Gold nanoparticles (Nanocs, NY, USA) with a varied diameter (15, 30, 50, 80, 100, 200, 400, 600 nm) were used to demonstrate ultrasonic-assisted nanoparticle separation on microfluidic devices. In the case of 60 nm/100 nm mixture, 10 µl of the stock solution of 60 and 100 nm (1.9×10^9/mL and 3.8×10^9/mL respectively) Au nanoparticles in 0.1 mM PBS were added into $1 \times$ PBS, and the final volume was brought up to 100 µl. The mixture was loaded into a sample reservoir of an assembled microfluidic device with a membrane filter for separation. (Fig. 4 (b)) The mixture was driven into the microfluidic device by the negative pressure generated by the syringe pump operating on "withdraw" mode. Flow velocity was set to 0.1 mL/h. The microfluidic device was irradiated with ultrasonic waves generated by the ultrasonic transducer during the separation. During the separation process, other inlets and outlets were closed than the waste port. Before collecting target particles, 0.1% Pluronic F108 solution was injected at 0.1 mL/h for 10 min as a washing buffer. Backwashing with the ultrasonic wave was performed to retrieve 60 nm gold nanoparticle (target) from the chamber region between two membrane filters. 60 nm gold nanoparticles (Au NP) were collected in either 0.1% F108 solution or PBS for downstream analysis. The retentate settled on the first membrane was collected by pipetting up and down several times for measurement.

2.5 Characterization of Populations of Nanoparticles

UV-Vis spectroscopy was used to characterize the populations of nanoparticles before and after the filtration process by quantifying the absorption intensity of each solution. Populations of nanoparticles were characterized by measuring peak absorbance and intensity wavelengths on a multimode plate reader (Perkin Elmer). The wavelengths of peak absorbance depend on the sizes of gold nanoparticles. Typically, peak absorbance occurs within 564–574 nm and 538–544 nm for 100 nm and 60 nm Au NP. Samples (Filtrates, retentates) collected from the microfluidic device after separation were analyzed within the 400–700 nm wavelength range, and the results were compared with that of the stock solution. Based on concentration and volume loaded, the recovery rate and sample loss were calculated.

To validate the filtration efficiency fluorescence image was obtained using a fluorescent microscope. 350 and 450 nm fluorescently labelled polystyrene nanoparticles were filtered on a microfluidic device incorporated with a 400 nm pore membrane filter to visualize NP adsorbed onto the membrane surface. The membrane was taken out of the device and investigated under a microscope. The 450 nm particles settled onto the membrane were considered sample loss, and the number of particles was counted automatically using Image J software.

In addition, particle size distribution was also determined by dynamic light scattering (DLS) using isolated filtrate and retentate prepared in 0.1% F108 solution. The distribution data were acquired and compared with the distribution data of each stock solution. All experiments were carried out at least 3 times.

3 Results and Discussion

3.1 Characterization of Microfluidic size-based NP Separation with Ultrasonic Irradiation

The efficiency of nanoparticle filtration using the microfluidic system with ultrasonic irradiation was evaluated with monodisperse 60 nm gold nanoparticles and a single track-etched polycarbonate membrane filter with an 80 nm pore size cut-off (Fig. 5). Twenty microliters of the gold nanoparticle stock solution were diluted with 80 µL of 0.1% F108 solution and placed into the loading reservoir. Filtration was performed both with and without ultrasonic irradiation to assess the efficiency of ultrasonic treatment. The results were analyzed using UV-Vis spectroscopy. To achieve a monodisperse target size, it is essential to maximize the recovery rate while ensuring that no detectable particles remain in the retentate solution. Recovery rates and losses were calculated by normalizing the absorbance profile of the feed solution. Without ultrasonic irradiation, significant sample loss was observed, likely due to particle adsorption onto the membrane surface during the process. The peak absorbance of the filtrate showed that only 21% of the input was recovered, resulting in a prolonged recovery rate. The peak absorbance of the retentate suggested that 17.9% of the input could not penetrate the membrane and was retrieved manually.

In contrast, with ultrasonic irradiation, a significant enhancement in the recovery rate was observed. The absorbance of the retentate solution was negligible, indicating that very few 60 nm particles remained in the solution. The recovery rate achieved with ultrasonic treatment was 70.6%, which is 3.9 times higher than without ultrasonic treatment.

3.2 Effect of Surface Treatment

In our initial attempt to determine the filtration efficiency of the microfluidic device, we found that efficiency is highly dependent on the membrane surface condition. When the sample volume passed through the membrane and the

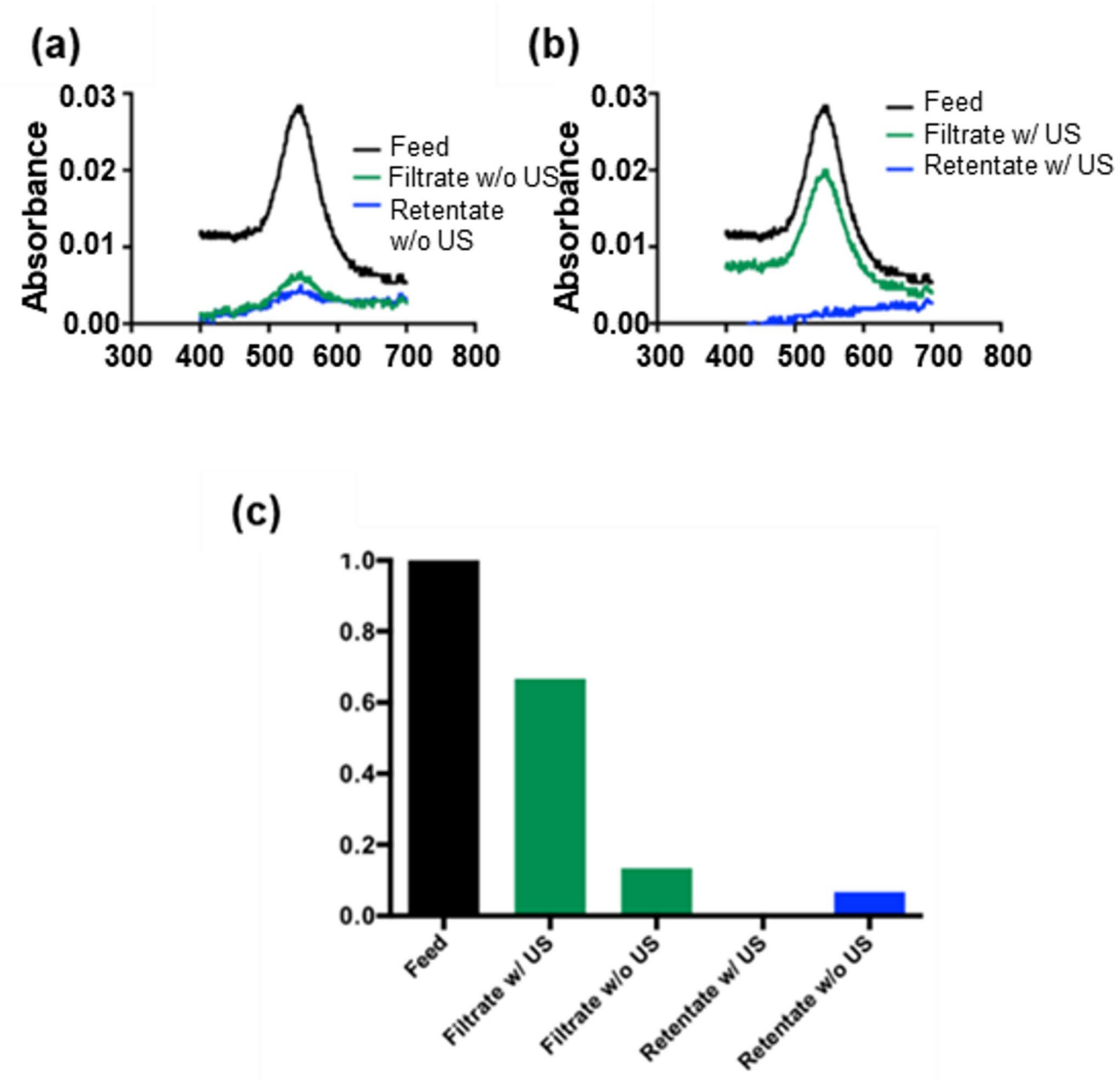


Fig. 5 60 nm Au NP filtration using membrane filter with 80 nm pore size cut-off embedded in the microfluidic size-based particle separation device. (**a**) The absorbance was measured using the feed, filtrate, and retentate sample collected after filtration without ultrasonic irradiation. (w/o US) (**b**) The absorbance results were compared to the case with ultrasonic irradiation (w/US). (**c**) In the presence of ultrasonic irradiation, 70.6% of input 60 nm particles were successfully collected, while 21% of input particles were collected without ultrasonic treatment

surface began to dry, the gold nanoparticles (Au NPs) that had settled on the membrane became compacted. This compaction, along with the formation of a cake layer by foulants, made it difficult to re-suspend the particles for downstream analysis, even with vigorous pipetting. To maximize efficiency and recovery, it is crucial to keep the membrane surface wet during and after filtration. This phenomenon was demonstrated using monodisperse fluorescently labeled polystyrene (PS) nanoparticles, which were visualized with a fluorescent microscope. The nanoparticles had a hydraulic diameter of 450 nm, while the membrane filter used for filtration had a pore size cut-off of 400 nm.

Figure 6 compares the removal rates between conditions with and without ultrasonic treatment, on both wet and dry surfaces. Figure 6(a) shows the 450 nm particles on the 400 nm filter surface after 100 µl of the sample had passed through. Under wet surface conditions (Fig. 6(b)-(c)), the effectiveness of ultrasonic cleaning was examined.

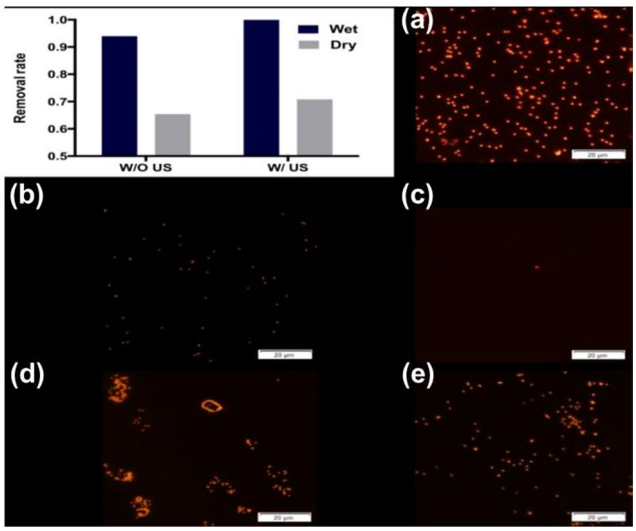


Fig. 6 Comparison of particle removal rate under different surface conditions (wet/dry). (**a**). 450 nm particles on a 400 nm filter after filtration. (**b**) and (**c**). Under wet conditions, most particles were removed with backflushing or ultrasonic cleaning, with no detectable particles remaining after ultrasonic treatment. (**d**) and (**e**). In dry conditions, significant fouling occurred

The results showed that most input particles were successfully removed from the filter surface through backflushing or pipetting. Without ultrasonic treatment, the loss was 5%, whereas no detectable nanoparticles remained on the surface after ultrasonic cleaning. This suggests that nanoparticles larger than the membrane's pore size tend to stay in suspension under wet conditions, and the cake layer formed during filtration is easier to remove with ultrasonic irradiation.

In contrast, when the membrane surface was allowed to dry, severe fouling was observed, indicating the irreversible formation of a cake layer with foulants (Fig. 6(d)-(e)). While ultrasonic irradiation improved the removal rate, significant losses were still detected. Specifically, 65% of input particles were removed without ultrasonic cleaning, compared to 70% with ultrasonic cleaning. This suggests that approximately 30% of nanoparticles larger than the pore size were likely adsorbed onto the membrane surface irreversibly under dry conditions. Therefore, keeping the membrane filter surface wet during and after filtration is essential for effective recovery of target particles, and ultrasonic cleaning further enhances particle removal from the surface.

To evaluate the effectiveness of the microfluidic device in sorting nanoparticles by size, we performed filtration of a 100 nm and 400 nm nanoparticle mixture and analyzed the particle size distribution using dynamic light scattering (DLS) (Fig. 7). The device was loaded with a mix of polystyrene particles of two different sizes and pressurized to facilitate size-based filtration. For the separation of 100 nm and 400 nm particles, we used 80 nm and 200 nm track-etched membrane filters. The filtrate was collected from the reservoir using backflushing combined with ultrasonic treatment.

Figure 7 illustrates the size distribution profiles of the original 100 nm and 400 nm stock solutions, the filtrate, and the mixture. Before filtration, we assessed the size distribution of the polydisperse mixture. The filtrate exhibited a size distribution profile similar to that of the original 100 nm stock solution, with no significant shift in peak wavelength or spectrum broadening. We compared the size distribution profile obtained from light scattering with the size estimated from absorbance spectra. The peak absorbance of the filtrate was approximately 70% of the stock solution's absorbance, with only slight variation in peak wavelength, indicating effective size discrimination and a high recovery rate.

3.3 Effect of Orientation of the Ultrasonic Treatment

We investigated the impact of ultrasonic transmitter orientation on the performance of the device in particle fractionation and recovery rate using 60 nm gold nanoparticles (Au NPs). The fractionation was performed with track-etched membrane filters featuring an 80 nm pore size cut-off. We tested the effect of the ultrasonic transmitter's orientation by positioning it either at the feed side or the permeate side of the device. As shown in Fig. 8, we investigated the effect of ultrasonic treatment orientation on the recovery rate. A 40 kHz, 40Vp-p ultrasonic wave was generated and focused on the membrane filters from either the permeate (clean fluid) side or the feed (sample fluid) side. Figure 8(a) illustrates the layout of the microfluidic particle filtration system with the embedded ultrasonic transmitter. The output voltage from the amplifier was set to 40 Vp-p. To assess the ultrasonic-assisted filtration performance, 50 µl of 60 nm Au NP stock solution was mixed with 50 µl of 0.1% F108 surfactant solution. Filtration was initiated by introducing 100 µl of this sample into the device. To maximize recovery, after the initial sample passed through, 100 µl of 0.1% F108 was reintroduced to collect residual particles in the collection reservoir. Following filtration, the collected samples were analyzed using a UV-Vis spectrophotometer, scanning the absorbance spectra in the 350–700 nm wavelength range. The results showed that the sample filtered with the ultrasonic transmitter positioned at the feed side achieved a higher recovery rate of 57% for the 60 nm Au NPs (Fig. 8(b)). In contrast, ultrasound irradiation at the permeate side resulted in a recovery rate of 48% from the same input sample.

In addition, the volumetric flow rate was monitored every 30 s up to 20 min using each transmitter configuration under the same pressure and input concentration condition. (Fig. 9) As a result, a similar trend was also seen in volumetric flow

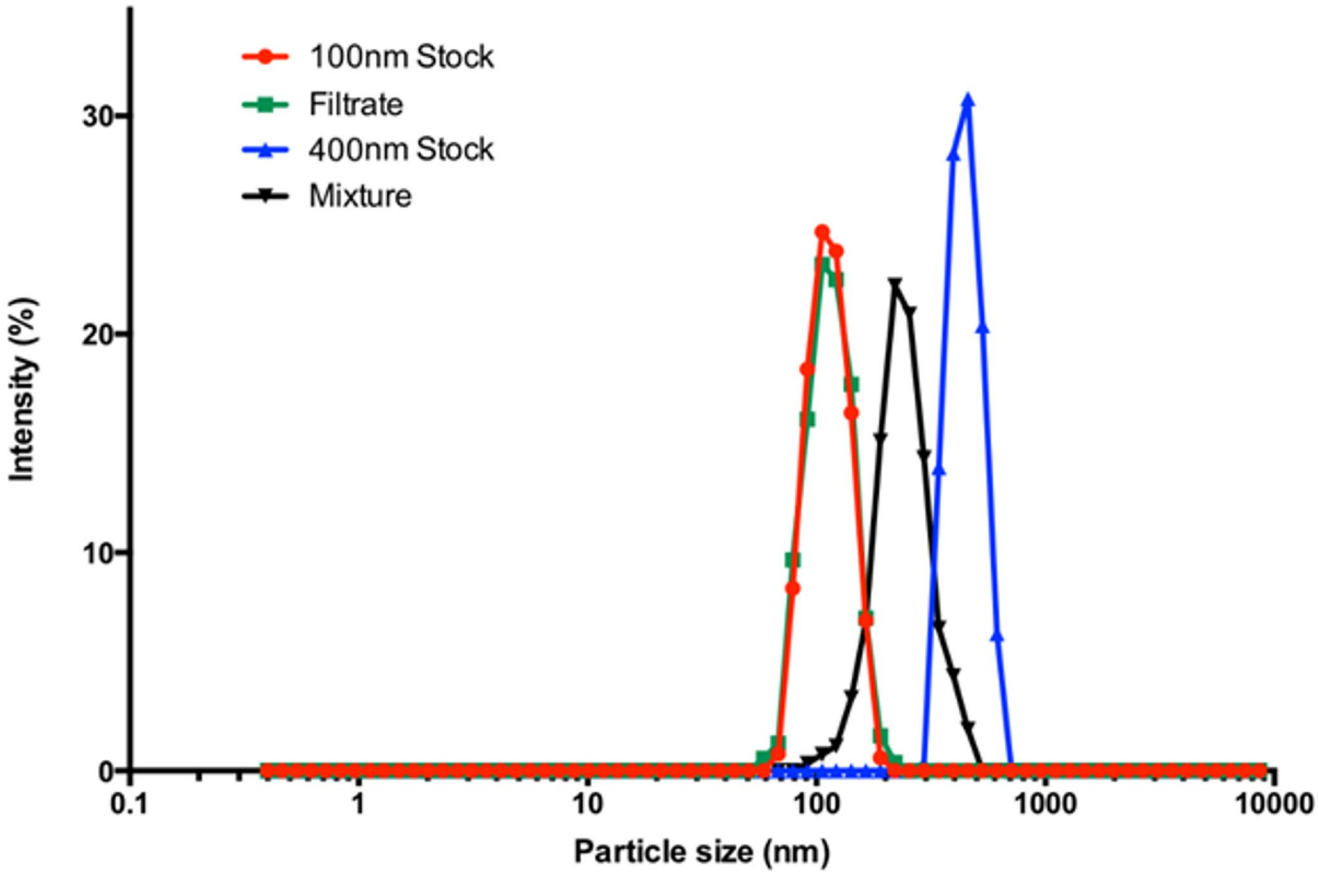


Fig. 7 Fractionation of 100 nm polystyrene NP from polydisperse mixture solution by using ultrasonic-assisted microfluidic particle sorting

rate results. The higher volumetric flow rate was achieved when ultrasound was irradiated onto the membrane surface from the feed side of the membrane. A significant decrease in flow rate occurred after 5 min filtration when ultrasound was irradiated from the permeate side of the membrane, indicating critical fouling of the membrane. Despite the decrease in the flow rate of ultrasound irradiation from the feed side, the flow rate stabilized after the initial 10 min separation process. On the other hand, flow rate consistently decreased in ultrasonic irradiation from the permeate side, showing a similar trend as with no ultrasonic treatment. The flow rate was double with ultrasonic irradiation compared to no ultrasonic treatment when the ultrasonic propagated from the feed side. According to the flow rate results, we assumed that the orientation of the ultrasonic transmitter affected the effectiveness of the ultrasonic treatment in preventing the formation of cake layer and fouling of membrane as well as recovery of the target particle.

4 Conclusions

The acustofluidics lab-on-a-chip (LOC) system for size-based nanoparticle separation using dead-end membrane filtration has demonstrated a remarkable leap in performance through ultrasonic agitation. Unlike conventional ultrasonic-assisted filtration methods, which often rely on complex macroscale systems, our approach integrates an ultrasonic transducer directly into a microfluidic setup, facilitating efficient nanoscale particle separation. With this innovative method, we successfully fractionated 60 nm gold nanoparticles from a mixed solution of 60 nm and 100 nm particles, using ultrasonic waves in the 28–40 kHz range. The system's agitation prevents cake layer formation and fouling on the membrane surface, significantly enhancing separation efficiency. Remarkably, the process, which takes approximately 10 min, achieved a 70% recovery rate for gold nanoparticles—an impressive improvement over non-ultrasonic methods.

While this study successfully demonstrates the promise of our acoustofluidics platform for nanoparticle separation, we acknowledge certain limitations and identify clear avenues for future work. Our current findings, particularly

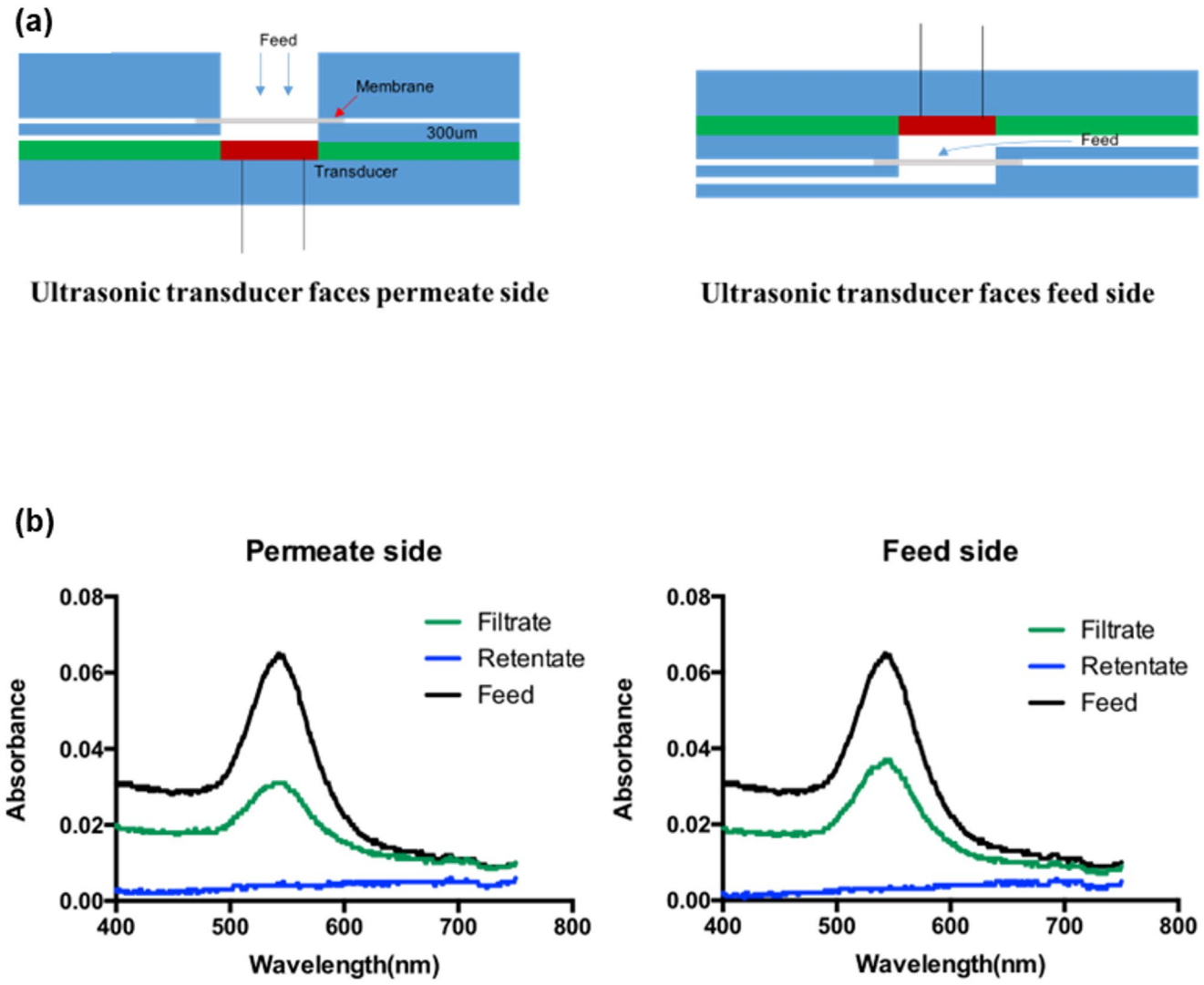


Fig. 8 Effect of the orientation of ultrasonic treatment on recovery rate. (**a**) Layouts of the microfluidic systems for particle filtration for ultrasonic treatment from the membrane filters' permeate side (left) and the feed side (right). The distance between the transducer and membrane remains 300 μm for the experiment. (**b**) Absorbance spectra of 60 nm Au NP collected in the filtrate solution by ultrasonic treatment from the permeate side (left) and feed side (right) of the membrane filters were compared with the absorbance using an original stock solution of 60 nm Au NP

the 70% recovery rate, are primarily based on 60 nm Au nanoparticles. Future research will focus on clarifying the scalability of these recovery rates to a broader range of biological targets, such as monosomes, and further optimizing the system to minimize sample loss. Additionally, to solidify the platform's advantages for point-of-care (POC) applications, future efforts will include rigorous comparative studies with existing separation techniques and validation experiments within complex biological matrices. These advancements will be crucial for fully realizing its potential in real-world POC settings.

This novel microfluidic LOC system offers substantial advantages over traditional size-based techniques, including: (1) Simplified fabrication with commercially available track-etched membranes, bypassing the need for complex microstructure fabrication; (2) Streamlined sample handling through automation; (3) High recovery rates, exemplified by the 70% recovery of 60 nm gold nanoparticles; (4) Elimination of additional chemical pretreatments thanks to membrane filtration; (5) Rapid and straightforward processing; and (6) Minimal sample dilution.

As this technology is still in its developmental phase, further system-level validation is needed for real-world applications. The next step involves testing the system for size-selective separation in biological samples, such as monosomes (~30 nm), to evaluate its potential for research and clinical use, particularly in ribosome profiling.

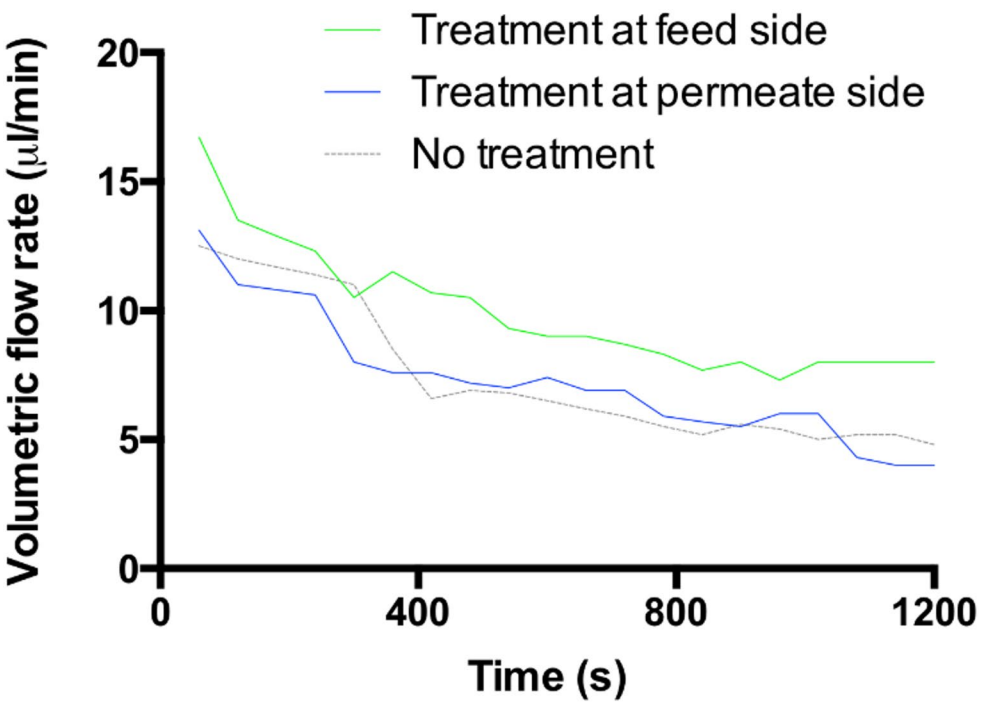


Fig. 9 Volumetric flow rate of sample filtered using microfluidic particle separation system as a function of filtration time

Supplementary Information The online version contains supplementary material available at https://doi.org/10.1007/s40684-025-00782-5.

Acknowledgements This work was supported by the Korea Institute of Energy Technology Evaluation and Planning (KETEP), the Ministry of Trade, Industry & Energy (MOTIE) of the Republic of Korea (No. 20194030202360), the MSIT(Ministry of Science, ICT), Korea, under the High-Potential Individuals Global Training Program) (2020-0-01580) supervised by the IITP(Institute for Information & Communications), Ralph W. and Grace M. Showalter Research Trust (No. 41001449), Clifford B. Kinley Trust, and Health of the Forces by Purdue University.

Author contributions JY and NK wrote the main manuscript text and prepared figures. HJC and YJY edit the manuscript and supervision the whole process. SJ, JN, IP and SL support gather resources. All authors reviewed the manuscript for final approval.

Funding Open Access funding enabled and organized by KAIST.

Declarations

Conflict of interest The authors declare no competing interests.

Open Access This article is licensed under a Creative Commons Attribution 4.0 International License, which permits use, sharing, adaptation, distribution and reproduction in any medium or format, as long as you give appropriate credit to the original author(s) and the source, provide a link to the Creative Commons licence, and indicate if changes were made. The images or other third party material in this article are included in the article's Creative Commons licence, unless indicated otherwise in a credit line to the material. If material is not included in the article's Creative Commons licence and your intended use is not permitted by statutory regulation or exceeds the permitted use, you will need to obtain permission directly from the copyright holder. To view a copy of this licence, visit http://creativecommons.org/licenses/by/4.0/.

References

1. Chan, W. X., Kim, N., Ng, S. H., & Yoon, Y. J. (2017). Acoustic energy distribution in microfluidics chip via a secondary channel. *Sensors and Actuators. B, Chemical, 252*, 359–366. https://doi.org/10.1016/J.SNB.2017.05.166
2. Kim, N., Chan, W. X., Ng, S. H., Yoon, Y. J., & Allen, J. B. (2020). Understanding Interdependencies between Mechanical Velocity and Electrical Voltage in Electromagnetic Micromixers. Micromachines 2020, Vol. 11, Page 636. 11, 636 https://doi.org/10.3390/MI11070636
3. Kim, N., Chan, W. X., Ng, S. H., & Yoon, Y. J. (2018). An acoustic micromixer using low-powered voice coil actuation. *Journal of Microelectromechanical Systems, 27*, 171–178. https://doi.org/10.1109/JMEMS.2017.2788566
4. Kim, N., Han, K., Su, P. C., Kim, I., & Yoon, Y. J. (2021 11:1). A rotationally focused flow (RFF) microfluidic biosensor by density difference for early-stage detectable diagnosis. Scientific Reports 11, 1–12 (2021). https://doi.org/10.1038/s41598-021-88647-0
5. Robertson, J. D., Rizzello, L., Avila-Olias, M., Gaitzsch, J., Contini, C., MagoÅ, M. S., Renshaw, S. A., & Battaglia, G. (2016). Purification of nanoparticles by size and shape. *Scientific Reports, 2016 6*(1), 6, 1–9. https://doi.org/10.1038/srep27494
6. Wu, M., Mao, Z., Chen, K., Bachman, H., Chen, Y., Rufo, J., Ren, L., Li, P., Wang, L., & Huang, T. J. (2017). Acoustic separation of nanoparticles in continuous flow. *Advanced Functional Materials*, *27*, 1606039. https://doi.org/10.1002/ADFM.201606039
7. Kowalczyk, B., Lagzi, I., & Grzybowski, B. A. (2011). Nanoseparations: Strategies for size and/or shape-selective purification of nanoparticles. *Current Opinion in Colloid & Interface Science, 16*, 135–148. https://doi.org/10.1016/J.COCIS.2011.01.004
8. Van Den Berg, A., Craighead, H., Yang, P., Lenshof, A., & Laurell, T. (2010). Continuous separation of cells and particles in

microfluidic systems. *Chemical Society Reviews*, *39*, 1203–1217. https://doi.org/10.1039/B915999C
9. Sajeesh, P., & Sen, A. K. (2014). Particle separation and sorting in microfluidic devices: A review. *Microfluid Nanofluidics*, *17*, 1–52. https://doi.org/10.1007/S10404-013-1291-9/FIGURES/85
10. Balyan, P., Saini, D., Das, S., Kumar, D., & Agarwal, A. (2020). Flow induced particle separation and collection through linear array pillar microfluidics device. *Biomicrofluidics*, *14*, 24103. https://doi.org/10.1063/1.5143656/134203
11. Huh, D., Bahng, J. H., Ling, Y., Wei, H. H., Kripfgans, O. D., Fowlkes, J. B., Grotberg, J. B., & Takayama, S. (2007). Gravity-driven microfluidic particle sorting device with hydrodynamic separation amplification. *Analytical Chemistry, 79*(4), 1369–1376. https://doi.org/10.1021/AC061542N
12. Kuntaegowdanahalli, S. S., Bhagat, A. A. S., Kumar, G., & Papautsky, I. (2009). Inertial microfluidics for continuous particle separation in spiral microchannels. *Lab on a Chip, 9*, 2973–2980. https://doi.org/10.1039/B908271A
13. Shi, J., Huang, H., Stratton, Z., Huang, Y., & Huang, T. J. (2009). Continuous particle separation in a microfluidic channel via standing surface acoustic waves (SSAW). *Lab On A Chip, 9*, 3354–3359. https://doi.org/10.1039/B915113C
14. Dalili, A., Montazerian, H., Sakthivel, K., Tasnim, N., & Hoorfar, M. (2021). Dielectrophoretic manipulation of particles on a microfluidics platform with planar tilted electrodes. *Sensors and Actuators. B, Chemical, 329*, Article 129204. https://doi.org/10.1016/J.SNB.2020.129204
15. Akbulut, O., MacE, C. R., Martinez, R. V., Kumar, A. A., Nie, Z., Patton, M. R., & Whitesides, G. M. (2012). Separation of nanoparticles in aqueous multiphase systems through centrifugation. *Nano Letters*, *12*, 4060–4064. https://doi.org/10.1021/NL301452X/SUPPL_FILE/NL301452X_SI_001.PDF
16. Arosio, P., Müller, T., Mahadevan, L., & Knowles, T. P. J. (2014). Density-gradient-free microfluidic centrifugation for analytical and preparative separation of nanoparticles. *Nano Letters*, *14*, 2365–2371. https://doi.org/10.1021/NL404771G/SUPPL_FILE/NL404771G_SI_001.PDF
17. Yeo, J. C., Kenry, Zhao, Z., Zhang, P., Wang, Z., & Lim, C. T. (2018). Label-free extraction of extracellular vesicles using centrifugal microfluidics. *Biomicrofluidics*, *12*, 24103. https://doi.org/10.1063/1.5019983/385682
18. Arnaud, I., Abid, J. P., Roussel, C., & Girault, H. H. (2005). Size-selective separation of gold nanoparticles using isoelectric focusing electrophoresis (IEF). *Chemical Communications*, *0*, 787–788. https://doi.org/10.1039/B413719A
19. Hanauer, M., Pierrat, S., Zins, I., Lotz, A., & Sönnichsen, C. (2007). Separation of nanoparticles by gel electrophoresis according to size and shape. *Nano Letters, 7*(9), 2881–2885. https://doi.org/10.1021/NL071615Y
20. Zhao, S., Wu, M., Yang, S., Wu, Y., Gu, Y., Chen, C., Ye, J., Xie, Z., Tian, Z., Bachman, H., Huang, P. H., Xia, J., Zhang, P., Zhang, H., & Huang, T. J. (2020). A disposable acoustofluidic chip for nano/microparticle separation using unidirectional acoustic transducers. *Lab on a Chip, 20*, 1298–1308. https://doi.org/10.1039/D0LC00106F
21. Latham, A. H., Freitas, R. S., Schiffer, P., & Williams, M. E. (2005). Capillary magnetic field flow fractionation and analysis of magnetic nanoparticles. *Analytical Chemistry*,*77*,5055–5062.
22. Shamloo, A., & Parast, F. Y. (2019). Simulation of blood particle separation in a trapezoidal microfluidic device by acoustic force. *IEEE Transactions on Electron Devices, 66*, 1495–1503. https://doi.org/10.1109/TED.2018.2889912
23. Gaborski, T. R., Snyder, J. L., Striemer, C. C., Fang, D. Z., Hoffman, M., Fauchet, P. M., & McGrath, J. L. (2010). High-performance separation of nanoparticles with ultrathin porous nanocrystalline silicon membranes. *Acs Nano*, *4*, 6973–6981. https://doi.org/10.1021/NN102064C/SUPPL_FILE/NN102064C_SI_001.PDF
24. Zhao, W., Lin, L., & Hsing, I. M. (2010). Nucleotide-mediated size fractionation of gold nanoparticles in aqueous solutions. *Langmuir, 26*(10), 7405–7409. https://doi.org/10.1021/LA9044489
25. De Jong, J., Lammertink, R. G. H., & Wessling, M. (2006). Membranes and microfluidics: A review. *Lab on a Chip, 6*, 1125–1139. https://doi.org/10.1039/B603275C
26. Noblitt, S. D., Kraly, J. R., VanBuren, J. M., Hering, S. V., Collett, J. L., & Henry, C. S. (2007). Integrated membrane filters for minimizing hydrodynamic flow and filtering in microfluidic devices. *Analytical Chemistry*, *79*, 6249–6254. https://doi.org/10.1021/AC070943F/SUPPL_FILE/AC070943FSI20070509_011646.PDF
27. Wei, H., Chueh, B. H., Wu, H., Hall, E. W., Li, C. W., Schirhagl, R., Lin, J. M., & Zare, R. N. (2011). Particle sorting using a porous membrane in a microfluidic device. *Lab on a Chip, 11*, 238–245. https://doi.org/10.1039/C0LC00121J
28. Fan, J. B., Luo, J., Luo, Z., Song, Y., Wang, Z., Meng, J., Wang, B., Zhang, S., Zheng, Z., Chen, X., & Wang, S. (2019). Bioinspired microfluidic device by integrating a porous membrane and heterostructured nanoporous particles for biomolecule cleaning. *ACS Nano, 13*, 8374–8381. https://doi.org/10.1021/ACSNANO.9B03918
29. Linkhorst, J., Beckmann, T., Go, D., Kuehne, A. J. C., & Wessling, M. (2016 6:1). Microfluidic colloid filtration. Scientific Reports 6, 1–8 (2016). https://doi.org/10.1038/srep22376
30. Belfort, G., Davis, R. H., & Zydney, A. L. (1994). The behavior of suspensions and macromolecular solutions in crossflow microfiltration. *Journal of Membrane Science, 96*, 1–58. https://doi.org/10.1016/0376-7388(94)00119-7
31. Shendruk, T. N., Tahvildari, R., Catafard, N. M., Andrzejewski, L., Gigault, C., Todd, A., Gagne-Dumais, L., Slater, G. W., & Godin, M. (2013). Field-flow fractionation and hydrodynamic chromatography on a microfluidic chip. *Analytical Chemistry, 85*, 5981–5988. https://doi.org/10.1021/AC400802G
32. Shin, K., Choi, J., Kim, Y., Lee, Y., Kim, J., Lee, S., & Chung, H. (2018). Feasibility study for combination of field-flow fractionation (FFF)-based separation of size-coded particle probes with amplified surface enhanced Raman scattering (SERS) tagging for simultaneous detection of multiple miRNAs. *Journal of Chromatography A, 1556*, 97–102. https://doi.org/10.1016/J.CHROMA.2018.04.057
33. Xu, J., Hong, H., Wang, Z., Sun, X., Wei, Y., & Liu, Y. (2024). Multiscale prototyping approach via in-situ switching electrohydrodynamics for flexible microfluidic design. *International Journal of Precision Engineering and Manufacturing-Green Technology, 11*(2), 353–364. https://doi.org/10.1007/s40684-023-00543-2
34. Kim, S., Kim, D. H., Kim, W., Cho, Y. T., & Fang, N. X. (2021). Additive manufacturing of functional microarchitected reactors for energy, environmental, and biological applications. *International Journal of Precision Engineering and Manufacturing-Green Technology*, *8*(1), 303–326. https://doi.org/10.1007/s40684-020-00277-5
35. Roos, M. M., Winkler, A., Nilsen, M., Menzel, S. B., & Strehle, S. (2022). Towards green 3D-microfabrication of Bio-MEMS devices using ADEX dry film photoresists. *International Journal of Precision Engineering and Manufacturing-Green Technology*, *9*(1), 43–57. https://doi.org/10.1007/S40684-021-00367-Y
36. Ingolia, N. T., Brar, G. A., Rouskin, S., McGeachy, A. M., & Weissman, J. S. (2012). The ribosome profiling strategy for monitoring translation in vivo by deep sequencing of ribosome-protected mRNA fragments. *Nature Protocols 2012*, *7*(7), 8. https://doi.org/10.1038/nprot.2012.086

37. Friend, J. (2023). Acoustofluidics. *Frontiers in Acoustics*, *1*, 1261027. https://doi.org/10.3389/FACOU.2023.1261027
38. Rasouli, R., Villegas, K. M., & Tabrizian, M. (2023). Acoustofluidics – Changing paradigm in tissue engineering, therapeutics development, and biosensing. *Lab on a Chip, 23*, 1300–1338. https://doi.org/10.1039/D2LC00439A
39. Sharma, A., Mondal, S., Mondal, A. K., Baksi, S., Patel, R. K., Chu, W. S., & Pandey, J. K. (2017). 3D printing: It's microfluidic functions and environmental impacts. *International Journal of Precision Engineering and Manufacturing-Green Technology*, *4*, 323–334. https://doi.org/10.1007/s40684-017-0038-6
40. Bachman, H., Fu, H., Huang, P. H., Tian, Z., Embry-Seckler, J., Rufo, J., Xie, Z., Hartman, J. H., Zhao, S., Yang, S., Meyer, J. N., & Huang, T. J. (2019). Open source acoustofluidics. *Lab on a Chip, 19*, 2404–2414. https://doi.org/10.1039/C9LC00340A
41. Rufo, J., Cai, F., Friend, J., Wiklund, M., & Huang, T. J. (2022 2:1). Acoustofluidics for biomedical applications. Nature Reviews Methods Primers 2, 1–21 (2022). https://doi.org/10.1038/s43586-022-00109-7
42. Kyllönen, H. M., Pirkonen, P., & Nyström, M. (2005). Membrane filtration enhanced by ultrasound: A review. *Desalination*, *181*, 319–335. https://doi.org/10.1016/J.DESAL.2005.06.003
43. Shi, X., Tal, G., Hankins, N. P., & Gitis, V. (2014). Fouling and cleaning of ultrafiltration membranes: A review. *Journal of Water Process Engineering*, *1*, 121–138. https://doi.org/10.1016/J.JWPE.2014.04.003

Publisher's Note Springer Nature remains neutral with regard to jurisdictional claims in published maps and institutional affiliations.